

Properties of graphite-stainless steel composite in bipolar plates in simulated anode and cathode environments of PEM fuel cells

RENATA WŁODARCZYK*

Department of Energy Engineering, Faculty of Environmental Engineering and Biotechnology,
Czestochowa University of Technology, ul. Brzeznicka 60a, 42-200 Czestochowa, Poland

The use of a graphite-stainless steel composite as bipolar plates (BP) in polymer electrolyte membrane fuel cells (PEMFCs) has been evaluated. The study covers measurements of mechanical properties, microstructural examination, analysis of surface profile, wettability, porosity and corrosion resistance of the composite. The corrosion properties of the composite were examined in $0.1 \text{ mol}\cdot\text{dm}^{-3} \text{ H}_2\text{SO}_4 + 2 \text{ ppm F}^-$ saturated with H_2 or with O_2 and in solutions with different pH: in $\text{Na}_2\text{SO}_4 + 2 \text{ ppm F}^-$ (pH = 1.00, 3.00, 5.00) at 80°C . The performed tests indicate that the graphite modified with stainless steel can be a good choice to be used as a bipolar plate in PEM fuel cells.

Keywords: powder metallurgy; sintering; graphite; bipolar plates; fuel cells; PEMFC

© Wrocław University of Technology.

1. Introduction

The polymer electrolyte membrane fuel cells are one of the promising options for portable, stationary power generators, or portable electronic devices [1]. The main components of fuel cells include electrolyte/membrane, electrodes (anode and cathode), bipolar plates (monopolar or bipolar) and end-plates (Fig. 1). Bipolar plates are a key element of PEMs, which account for 40 – 50 % cost and 60 – 80 % weight of the whole fuel cell stack [2]. Mass distribution of a generator weighting 24 kg, with a capacity of 33 kW is shown in Fig. 1A.

Respectively to the mass distribution of the individual components of the cell, the fuel cell should be light and cheap. Graphite is an excellent material for bipolar plates in PEM due to its great corrosion resistance, thermal resistance, high electrical conductivity but the fragile structure of graphite creates difficulty during its manufacturing.

Using BP materials in low-temperature fuel cell production requires consideration of the following factors: density, electrical conductivity, me-

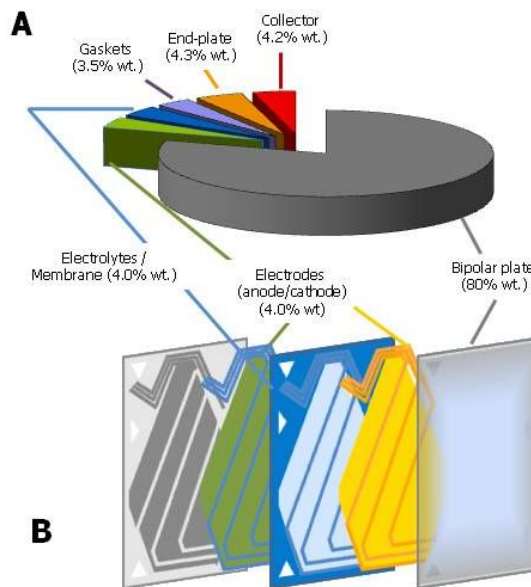


Fig. 1. A – The mass fraction of each component in the cell; B – Construction of a single fuel cell.

chanical properties, corrosion, chemical and thermal stability, gas permeability and manufacturing process [3]. The target material properties, including physical, mechanical and electrical properties,

*E-mail: rwlodarczyk@is.pcz.czest.pl

reported by DOE (Department of Energy, USA), used in BPs are presented in Table 1. Thin metal sheet is a suitable material for a bipolar plate. The metals used for the construction of a low-temperature fuel cell cover include nickel, titanium and coatings made based on these metals [4–7]. In [8], the possibility of using aluminum as a cheaper coating was studied. However, in the working environment of a fuel cell, oxidized aluminum and the products of the process contaminate the membrane. Alloys reported by Nikam et al. [9, 10] have high thermal conductivity and electrical and chemical stability as well as easier production with all advantages of copper. On the other hand, highly dense copper and its alloys disqualify these materials in the fuel cells.

The most common material in the group of metallic materials is stainless steel. It presents such qualities as high strength, low gas permeability, diversity of alloying elements and, above all, low production costs. Availability of stainless steel and the low cost of production are its advantages. It can be easily shaped into the form of plates of a thickness as low as 0.2 to 1 mm, suitable for the fabrication of channels in mono- or bipolar covers. The possibility of producing thin plates is associated with a high material density (density of approximately $7.80 \text{ g}\cdot\text{cm}^{-3}$), which unfortunately is a disadvantage in these applications. Austenitic steels are usually passivated in the PEM cells working environment [11, 12]. The significant influence of the chemical composition of stainless steel has also been discussed in papers [13–15]. Table 1 shows the properties of steel 316L on the basis of literature. According to the information, the 316 stainless steel belongs to a group of wettable materials and the ICR at a pressure of 1.4 MPa is in a range between 70 and 230 $\text{m}\Omega\cdot\text{cm}^2$, therefore, it does not apply to DOE requirements ($<20 \text{ m}\Omega\cdot\text{cm}^2$). Due to the changing environment in the fuel cell operating conditions, steel was tested in solutions of various concentrations of the acid with reference to the presence of fluoride ions from the electrolyte or pure acid. Steel corrosion current density in a sulphuric acid VI varied over a wide range from a few to tens of $\text{mA}\cdot\text{cm}^{-2}$. Comparing the properties of graphite, in terms of its application for the con-

struction of low-temperature fuel cell covers, the ICR and corrosion current density meet the requirements of DOE in 2011 (Table 2).

Following the recent reports and features, which are characteristic of carbon-based composites, the next step in the way of material requirements for 2017 will be a study on the construction or use of already existing materials with the following composition: graphite-polymer, carbon fiber-polymer fibers, etc. The most popular materials of bipolar plates, besides graphite, are metallic materials or composites based on carbon: carbon-carbon composites [25, 26], carbon-polymer composites [27], and carbon coated metal [27–30]. Metallic bipolar plates provide many advantages such as cheaper material cost, high thermal and electrical conductivity, variety of manufacturing processes and excellent mechanical properties. The advantages and disadvantages of graphite and metallic BP are depicted in Table 2.

In order to improve the mechanical properties of graphite without affecting its corrosion resistance, graphite-SS composite has been proposed.

The composite bipolar plate is a promising alternative to graphite; graphite-stainless steel (SS) composite may greatly improve the mechanical properties of graphite and corrosion resistance of SS in PEM environments. Two main fabrication methods for graphite composite bipolar plates are injection molding and compression molding [31–33] used to produce the composite by powder metallurgy technology.

The technology used in this study makes possible to determine the effect of compaction and sintering on the product properties. Finding the relationship between the technological parameters and properties of sinters allows obtaining materials with the desired mechanical properties and resistance to corrosion. The investigations of sintered stainless steel confirmed that the use of suitable parameters of compaction pressure and sintering atmosphere ensures obtaining materials with controllable density, pore and grain size and that a suitable chemical composition of powders allows for obtaining sinters with the desired functional properties [15, 16].

Table 1. Selected properties of the materials most frequently used for the construction of BP.

Materials	Contact angle [deg]	ICR at 1.4 MPa [mΩ·cm ²]	I_{corr} [A·cm ⁻²]	Corrosion environments	Literature
316 SS	–	125	approx 400×10^{-6}	1 M H ₂ SO ₄ + 2ppm HF, T = 80 °C	[16]
316 SS	–	approx 250	7×10^{-5}	SO ₄ ²⁻ , pH 2, T = 80 °C	[17]
316L SS	–	–	approx 9×10^{-6}	0.5M H ₂ SO ₄ , T = 70 °C	[18]
316L SS	–	–	40×10^{-6}	0.1 M H ₂ SO ₄ , T = 70 °C	[19]
			4×10^{-6}	0.1 M H ₂ SO ₄ , T = 20 °C	
316L SS	73	70	approx 5×10^{-5}	0.5 M H ₂ SO ₄ + 5 ppm F ⁻ , T = 70 °C	[20]
316L SS	48	230	2.4×10^{-5}	1 M H ₂ SO ₄ + 5 ppm F ⁻ , T = 70 °C	[21]
Graphite	–	2	3.8×10^{-6}	0.5 M H ₂ SO ₄ + 200 ppm HF, T = 20 °C	[22]
Graphite	80	20	–	–	[23]
Graphite	–	13	1.7×10^{-6}	1 M H ₂ SO ₄ + 2 ppm HF, T = 80 °C	[24]

Table 2. Advantages and disadvantages of graphite and metallic BP.

BP material	Advantages	Disadvantages	DOE, 2011 status
Poco graphite	– Corrosion resistance – Low ICR – High power density	– Porous – Poor machinability – Brittle – Relatively expensive	– Density <2.0 g·cm ⁻³ – Electrical conductivity >100 S·cm ⁻¹ – Contact resistance @ 1.4 MPa <20 mΩ·cm ² – Electrical resistivity: low as possible
Metal	– None porous – High electrical and thermal conductivity – Good machinability – Relatively inexpensive	– Corrode in acidic media – High ICR	– Corrosion resistance <16 × 10 ⁻⁶ A·cm ⁻² – Hydrogen permeability <2 × 10 ⁻⁴ cm ³ (s·cm ²) ⁻¹ – Thermal conductivity >10 W (m·K) ⁻¹ – Tensile strength >41 MPa – Flexural strength >50 MPa – Shore hardness >40 – Hydrophobicity: contact angle >90°

The paper presents the results of investigation on graphite-stainless steel composites, made by powder metallurgy methods, for bipolar plates applications. The plates made from the composites have improved characteristics in comparison to the plates made only of graphite or stainless steel material.

2. Experimental part

2.1. Materials for experiment

Stainless steel powder and graphite powders were manufactured by Höganäs (Sweden), and by Schunk Kohlenstofftechnik GmbH (Germany), respectively. Water atomized 316LHD (HD – high

density) steel and graphite powders were used to prepare a mixture (20 % wt. 316LHD). The mixed powder was compacted at 700 MPa by axial compression and then sintered at a temperature of 1150 °C ± 10 °C in vacuum. A sample was obtained in the form of tablets of 50 mm diameter and of about 4.80 mm thickness. The density, porosity and specific surface area were measured using a mercury porosimeter PoroMaster 33. The particle size distribution of the powders was measured by determining the diameter of the infrared beam (Kamika).

Graphite and SS powders showed a large difference in surface area and thus, the open porosity of the powder particles. Density of 316LHD

powder was 2 times higher than the density of graphite powder. The distribution size of graphite powder is shown in Table 3. About 97 % of particles have an average particle diameter below 60 μm . However, the number of particles with an average diameter of less than 10 μm is ca. 25 %. In SS powder the number of particles with a diameter of less than 60 μm is ca. 50 %.

The chemical composition of the powders is shown in Table 4. The chemical analysis was carried out using a spectrometer XRF (Rigaku) – model ZSX-Primus II. Fig. 2 shows the morphology of the powders. The graphite powder consists of particles with sharp edges. The powder is contaminated (about 0.05 %), as observed in the analysis of chemical composition. This small amount of various metals comes from the ash contained in graphite powders [34]. The steel powder, 316LHD, consists of irregularly shaped particles of various sizes. There is a single spherical particle. The powder is chemically uniform.

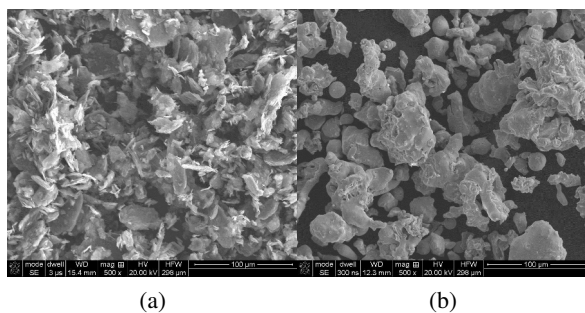


Fig. 2. Powders morphology, (a) graphite powder, (b) 316LHD steel powder.

2.2. Methodology

Density, porosity and specific surface area measurements of the composite were carried out using a mercury porosimeter PoroMaster 33 supported by Quantachrome Instruments software for Windows.

A compression test was performed on a universal testing machine INSTRON 8501 with an appropriate computer software, equipped with a strain gauge force measurement head, type 2518-103 No. 791 of the UK ± 5 kN. A pressure test was carried out at a speed of the actuator of 1 mm/min. During

the tensile test, the computer recorded changes in the value of the loading force and the displacement of the actuator of the testing machine.

In order to determine the degree of wetting, 3 μl of water was dropped on the surface of the graphite-stainless steel composite. The images of the material with a water drop were analyzed by a MicroCapture microcamera and special software for microimage analysis.

Measurements of interfacial contact resistance (ICR) between the surfaces of diffusion layer (GDL, usually carbon paper) and bipolar plates (BP) were carried out according to the methodology used by Zhang et al. [35]. Techniques of measurement of interfacial contact resistance have been broadly discussed in the studies [36, 37].

The analysis of the geometrical structure of the surface of the sinter was made using a profilographometer PG 1C working in a modular system TOPO 01. On that basis, the analysis of the surface was carried out, including height feature of profile R_a .

During the operation of PEM fuel cells, the ionic exchange membrane may dissolve acidic ions such as SO_4^- , SO_3^- , and HSO_4^- and F^- ions [38]. Products of corrosion of BP materials might poison the catalysts and decrease the efficiency of the fuel cell [39–41]. The working electrode was based on composite, the reference electrode was based on a saturated calomel electrode (SCE), and the auxiliary electrode was based on a Pt wire. Potentiokinetic curves were recorded after 10 seconds from the moment of putting the working electrode in the solution. The electrochemical measurements station was based on CHI 1140 (CH Instruments). Potentiokinetic testing was carried out at a scan rate of $5 \text{ mV}\cdot\text{s}^{-1}$.

3. Results and discussion

Properties of the obtained composite: graphite + 20 % 316L/700 are presented in Table 5. Steel powder particles were packed during pressing and sintering between particles graphite powder. The consequence of sintering two powders with different properties (density, specific surface area) gave

Table 3. Properties of powders used for sintering.

	Density [g·m ⁻³]	Specific surface area [m ² ·g ⁻¹]	<10 μm [%]	<20 μm [%]	<60 μm [%]
Graphite powder	2.23	7.12	24.49	51.86	96.95
316LHD powder	5.67	0.25	0.64	4.27	50.48

Table 4. Chemical composition of powders used for sintering (wt.%).

	[%]	[%]	Si [%]	Al [%]	Mo [%]	Ni [%]	Ti [%]	Fe [%]	Mn [%]	Cr [%]	C [%]
Graphite powder	S = 0.0076	P = 0.0004	0.0057	0.0027	0.0014	0.0046	0.0092	0.014	–	–	99.95
316LHD powder	O = 0.20	N = 0.03	0.25	0.213	2.62	12.25	–	67.76	0.06	16.63	0.02

the estimated value of specific surface area of the sinter of 3.29 m²·g⁻¹.

Table 5. Physical, mechanical and surface properties of composite graphite+20 % 316L/700.

	Graphite+20 % 316L/700
Density [g·cm ⁻³]	3.886
Hardness HBW 2,5/30/10	143.82
Compressive strength [MPa]	7.9
Porosity [%]	10.69
Specific surface area [m ² ·g ⁻¹]	3.29
Contact angle [deg]	124
ICR @ 1.4 MPa [mΩ·cm ²]	17.0
R _a [μm]	2.15

3.1. Surface properties

The microstructure of sintered graphite steel was porous as a result of the applied manufacturing technology – powder metallurgy method. We can observe the pores of the sizes of mesopores and macropores (Fig. 3). Distribution of pores in the graphite-stainless steel composite is shown in Fig. 4b. Micropores and mesopores determine the size of the inner surface and play an important role in adsorption processes. Macropores act as transport routes for accessing smaller pores (transporting pores) [42]. According to IUPAC (International

Union Pure and Applied Chemistry) the micropores have a diameter of <0.002 μm, mesopores have a diameter between 0.002 – 0.050 μm and macropores: >0.050 μm [43]. Knowledge of the nature of porous material brings various possibilities of materials application for diffusion layers, porous membranes, bipolar plates in fuel cells [44–46]. The specific surface area of the sintered composite is ca. 3.25 m²·g⁻¹ (Fig. 4a).

The available literature reports that wettability and contact resistance depend on surface geometry [47, 48]. A drop of a liquid, depending on a structure and profile of a rough hydrophobic surface, may be distributed homogeneously, or heterogeneously, leaving a space between the liquid and the solid. The surface roughness is very important from the point of view of surface contact resistance. Uneven, rough surfaces have a small share of contact area and thus, a high ICR value. To get the lower ICR materials for fuel cell covers, they must be polished [49]. Also graphite, as a highly porous material must be properly processed to obtain a minimum value of roughness parameters [50, 51]. Considering the strong influence of surface roughness on the other properties, geometric parameters of the sintered surface structure were analyzed.

During the whole operation, the fuel cell elements were in permanent contact with water (at the cathode side, water was generated and mixed with humidified gases to prevent dehydration of the

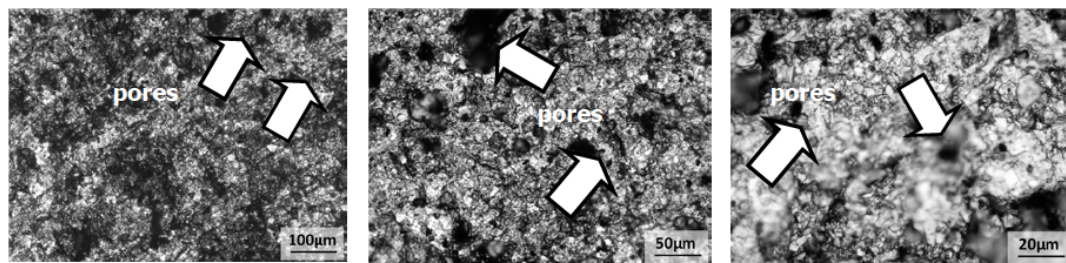


Fig. 3. Microstructures of graphite-stainless steel composite.

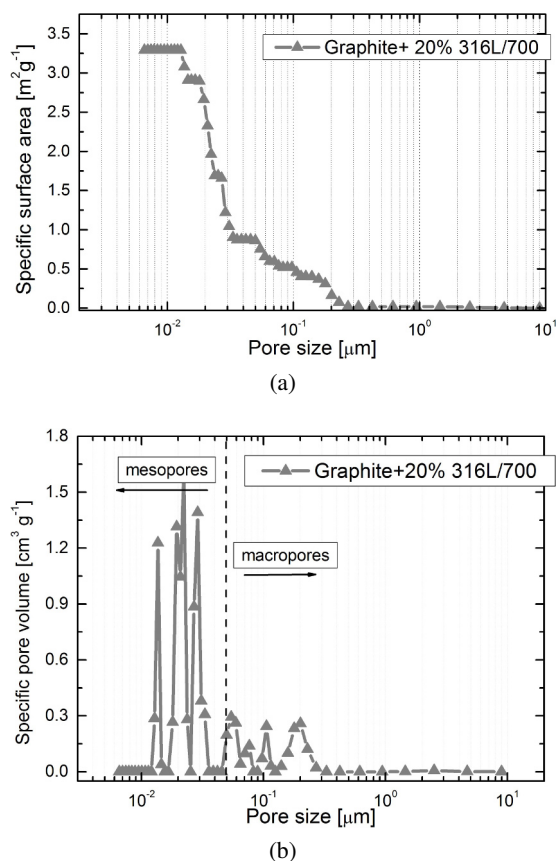


Fig. 4. Specific surface area (a) and specific pore volume (b) versus pore size in graphite-stainless steel composite.

membrane). If liquid water accumulates in the cell, the cell surface (especially the BP) hinders an access of the reaction gases to the electrodes. Water also accelerates the corrosion of the steel cell components. Accordingly, the degree of moisture in the cell is very important. Because of the cumulated water generated in the fuel cell, the cover materi-

als need to have non-wettable surfaces (hydrophobic). The composite is hydrophobic, when the Θ is higher than 90° (Table 4). Hydrophobic composite reduces, to some extent, the corrosion rate of the material in the fuel cell operating conditions.

One of the important properties of bipolar plates in PEM fuel cells is low interface contact resistance and high conductivity in order to minimize ohmic losses. According to DOE, the ICR value should be less than $20 \text{ m}\Omega\cdot\text{cm}^2$ at 1.4 MPa (Table 5). The ICR values of graphite-316L composite, where stainless steel has a function of compaction force generator (Fig. 5), at $140 \text{ N}\cdot\text{cm}^{-2}$ compaction force is around $17 \text{ m}\Omega\cdot\text{cm}^2$. For comparison, the ICR for sintered stainless steel 316L was ca. $55 \text{ m}\Omega\cdot\text{cm}^2$ with R_a $4.67 \mu\text{m}$ [16].

The electrical sheet resistance is very important for electrical properties of materials for bipolar plates production. Based on reported data, the electrical resistance measured by four-probe technique, gave results of $62 \text{ m}\Omega\cdot\text{cm}$, and $47 \text{ m}\Omega\cdot\text{cm}$, for graphite, and 316L SS, respectively [29]. In this report the electrical resistance of graphite-stainless steel composite was not tested. It can be assumed that graphite modified with SS will have lower electrical resistance in comparison with bare stainless steel. Composite with low electrical resistivity can reduce ohmic losses in fuel cells.

3.2. Microstructural analysis

The morphologies of graphite-stainless steel composite are shown in Fig. 6a. Based on the analysis of phase composition in the composite, austenitic phase of CrFeNi, crystallizes in a body-centered cubic cell with $a = 3.591 \text{ nm}$. The

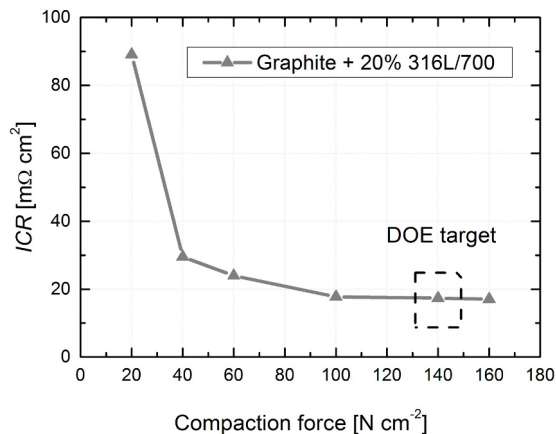


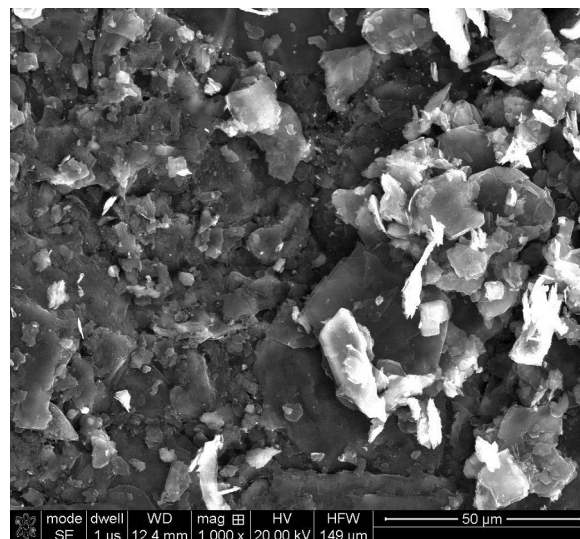
Fig. 5. Interfacial contact resistance for graphite-stainless steel composite depending on compaction force.

emerged peaks originate from hexagonal graphite, $a = b = 0.245$ nm, $c = 0.669$ nm, $\alpha = \beta = 90^\circ$, $\gamma = 120^\circ$ (Fig. 6b). Analysis of the chemical composition of a single crystallite of the composite material proved the austenite phase as well as carbon occurrence in the graphite form.

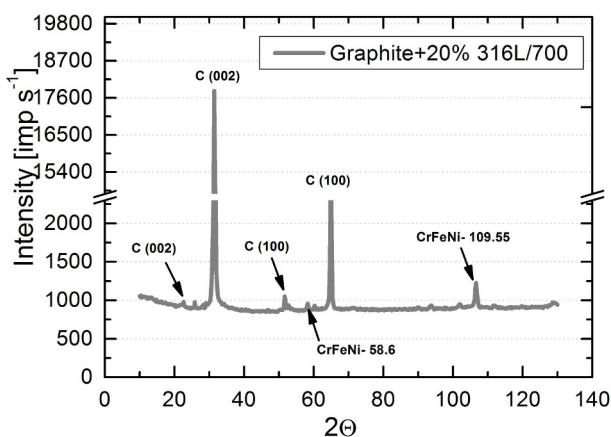
In order to determine the chemical composition of the composite, qualitative EDS (Energy Dispersive Spectroscopy) analysis was used. (Fig. 7).

3.3. Corrosion resistance

Fig. 8a shows the potentiokinetic curves of the graphite-stainless steel composite in simulated PEMFC solution (saturated with H_2 or with O_2). The corrosion potential of the sample is equal for both anode and cathode: in anode environment (solution saturated with H_2) $E_{corr} = ca. -0.32$ V vs. SCE, and in cathode environment (solution saturated with O_2) $E_{corr} = -0.33$ V vs. SCE. In oxygen medium, composites are passivated, which considerably reduces the rate of corrosion process in the active range (see the values of parameters i_{corr} and polarization resistance R_p in Table 6). The dynamic polarization tests (potentiokinetic tests) of graphite-SS composite behavior in PEMFC conditions confirm the formation of a passive area but the passive layer is not stable enough to reduce the current value in the range of 0.0V vs. SCE to 0.8V vs. SCE up to the value equal to or lower than i_{corr} .



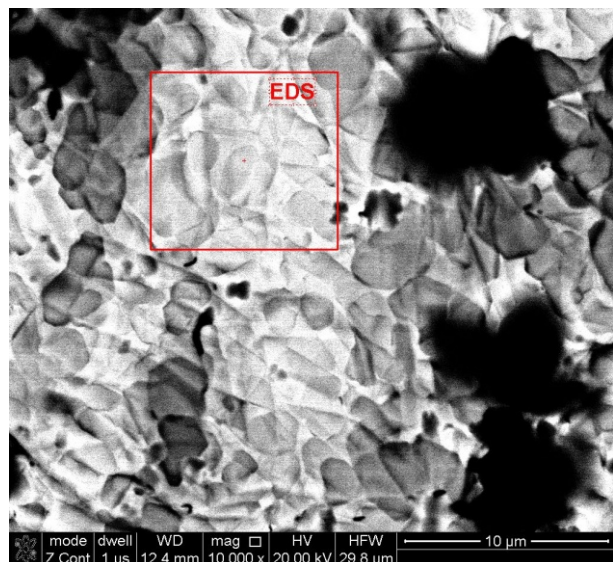
(a)



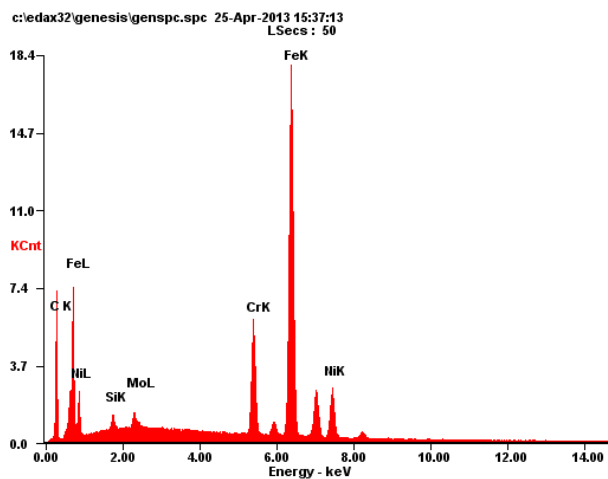
(b)

Fig. 6. SEM analysis (a) and diffractogram (b) of graphite-stainless steel composite.

The behavior of a curve registered in the solution saturated with oxygen shows a passive range of initial passivation at 0.4V vs. SCE [52]. Fig. 8a (inset) presents a polarization curve registered for the passivated steel. The a – b section corresponds to the area of active metal solubilisation. After reaching the potential of initial passivation (E_p , i_p), a passive layer is created on the metal surface. Current density decreases until it reaches the value even lower than i_{corr} and then it stabilizes. Further increase in the potential does not cause considerable changes in current density until the potential of transpassivation (point d) is reached, i.e. remod-



(a)

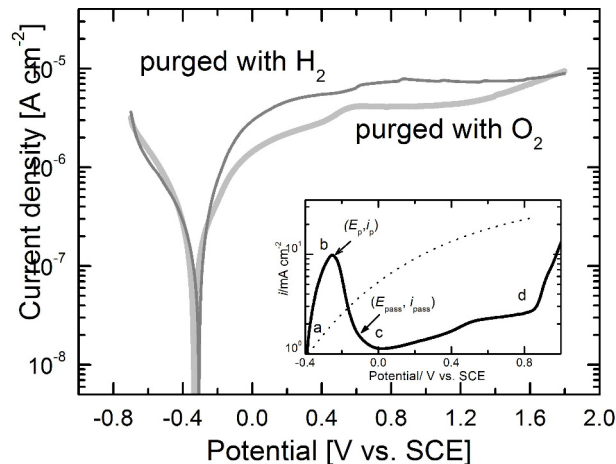


(b)

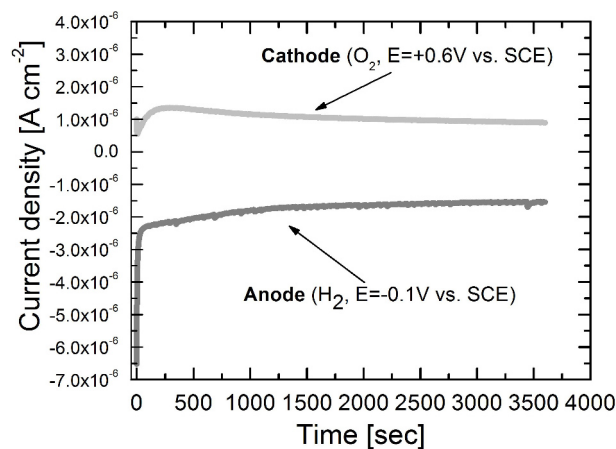
Fig. 7. SEM image (a) and EDS spectrum (b) of graphite-stainless steel composite.

elling of a passive layer. The dashed line represents potentiokinetic curves observed for non-passivated metal.

Current density versus time can be a measure of material durability at potential values, where the processes of hydrogen oxidation (-0.1 V vs. SCE) and oxygen reduction (0.6 V vs. SCE) occur (Fig. 8b). One can assume that the lower anode current density at the given potential and the longer time of 'protection' are, the better is corrosion resistance of a material. In order to determine



(a)



(b)

Fig. 8. Corrosion tests of graphite-stainless steel composite in $0.1 \text{ mol} \cdot \text{dm}^{-3} \text{ H}_2\text{SO}_4 + 2 \text{ ppm F}$, purged with O_2 or with H_2 , at $T = 80^\circ \text{C}$, (a) potentiokinetic curves and (b) potentiostatic curves.

the durability of the composite, chronoamperometric curves for the analyzed graphite-SS composite were registered. The anode current at the beginning of the test was about -6.5×10^{-6} $\text{A} \cdot \text{cm}^{-2}$ and then it stabilized at -1.6×10^{-6} $\text{A} \cdot \text{cm}^{-2}$. The obtained chronoamperometric curves for the composite (Fig. 8b) demonstrate a characteristic plateau after exceeding 100 seconds of exposure to the corrosion solution. In case of simulated cathode conditions (O_2), the current density has stabilized at 1.26×10^{-6} $\text{A} \cdot \text{cm}^{-2}$. This value is almost equal to the value obtained from the potentiokinetic tests

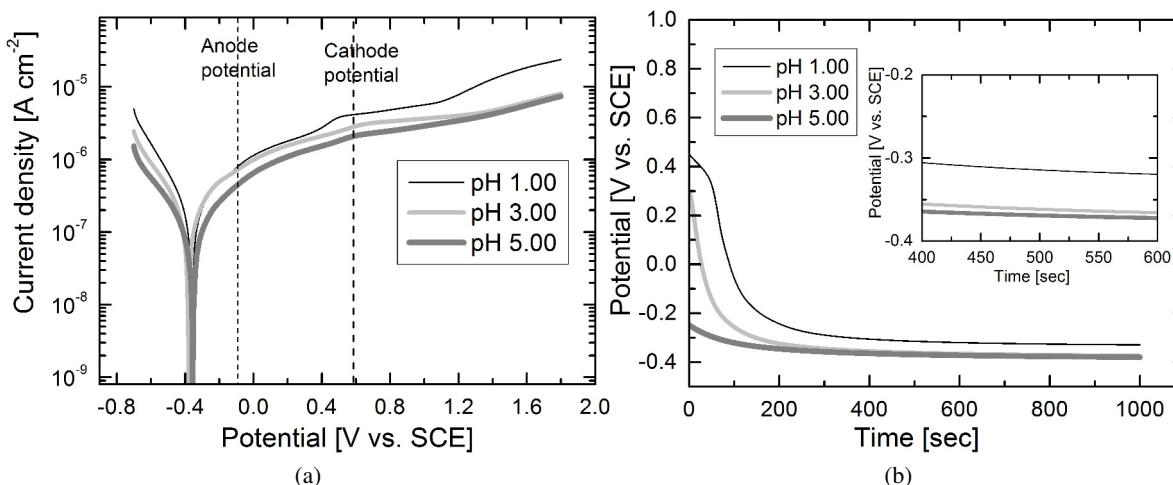


Fig. 9. Corrosion tests of graphite-stainless steel composite in $0.1 \text{ mol}\cdot\text{dm}^{-3} \text{ Na}_2\text{SO}_4 + 2 \text{ ppm F}^-$ at $T = 80 \text{ }^\circ\text{C}$, and pH values of 1.00, 3.00, and 5.00, (a) potentiokinetic curves (b) open circuit potential.

Table 6. Corrosion parameters obtained from potentiokinetic curves in Fig. 8a.

	Anode (purged with H_2)	Cathode (purged with O_2)
E_{corr} [V]	-0.322	-0.331
i_{corr} [$\text{A}\cdot\text{cm}^{-2}$]	2.67×10^{-7}	3.48×10^{-7}
i at -0.1 V vs. SCE [$\text{A}\cdot\text{cm}^{-2}$]	2.04×10^{-6}	-
i at 0.6 V vs. SCE [$\text{A}\cdot\text{cm}^{-2}$]	-	4.06×10^{-6}
R_p [$\text{k}\Omega\cdot\text{cm}^2$]	391	434

($4.06 \times 10^{-6} \text{ A}\cdot\text{cm}^{-2}$). On the basis of the potentiostatic tests we can make the following conclusion: the negative current provides cathode protection of BP material and the positive current appears because of the composite corrosion.

In order to check the corrosion resistance of the composite, the potentiodynamic curves were recorded in the solution of the following pH values: 1.00, 3.00, 5.00 (Fig. 9a). The corrosion potential of the composite has not significantly changed with pH of the solution. We can observe some differences in current density at anode and cathode potentials. The electrochemical parameters obtained from the potentiokinetic curves are shown in Table 7. The higher the value of polarization resistance, the higher material corrosion resistance. The highest corrosion resistance of the composite was obtained in solution of pH 5.00. Fig. 9b presents open circuit potential versus time in different pH. At free corrosion potential, corrosion oc-

curred faster in acidic solution (with pH 1.00) than in pH 5.00 solution.

The corrosion properties in anode and cathode environments meets the DOE's 2020 technical targets independently of pH of solution during operating of PEM fuel cells.

4. Conclusions

Except for a number of materials used for bipolar plates, the use of graphite modified with stainless steel seems to be very interesting. Application of the methods of powder metallurgy allows for controlling the density of the manufactured materials as well as their porosity, i.e. characteristics, which, in the case of bipolar plates in fuel cells, affect e.g. material heat capacity, heat and electrical conductivity, resistance to cracking as well as strength and plasticity. The graphite-stainless steel composite made in this investigation showed

Table 7. Corrosion parameters obtained from potentiokinetic curves in Fig. 9a.

	pH 1.00	pH 3.00	pH 5.00
E_{corr} [V]	-0.361	-0.374	-0.353
i_{corr} [$A \cdot cm^{-2}$]	2.52×10^{-7}	1.58×10^{-7}	8.02×10^{-8}
i at -0.1 V vs. SCE [$A \cdot cm^{-2}$]	8.35×10^{-7}	7.52×10^{-7}	4.47×10^{-7}
i at 0.6 V vs. SCE [$A \cdot cm^{-2}$]	3.98×10^{-6}	2.91×10^{-6}	2.13×10^{-6}
R_p [$k\Omega \cdot cm^2$]	459	587	995

properties, which met the requirements formulated by the DOE. The density of the composite was below $2 \text{ g} \cdot \text{cm}^{-3}$, ICR at $140 \text{ N} \cdot \text{cm}^{-2}$ below $20 \text{ m}\Omega \cdot \text{cm}^2$, and the material was characterized by low corrosion resistance. Based on the analysis of the contact angle, the composite materials were classified as non-wettable (hydrophobic).

The corrosion properties in anode and cathode environments met the DOE's 2020 technical targets. Tests performed proved that the graphite-SS composite can be a suitable choice for the use as a bipolar plate in PEM fuel cells.

Acknowledgements

I would like to thank Professor Z. Bojar for the opportunity to study in the Department of Advanced Materials and Technology, and Dr. D. Siemiaszko and Dr. D. Zasada for their assistance, and other colleagues from the Department for fruitful discussions.

References

- [1] KIRUBAKARAN A., JAIN S., NEMA R.K., *Renewable and Sustainable Energy Rev.*, 13 (2009) 2430.
- [2] COOPER J.S., *J. Power Sources*, 129 (2004) 152.
- [3] LARMINIE J., DICKS A., *Fuel Cell Systems Explained*, Wiley & Sons, Ltd., 2003.
- [4] SHOW Y., *Surf. Coat. Technol.*, 202 (2007) 1252.
- [5] SHOW Y., MIKI M., NAKAMURA T., *Diamond Relat. Mater.*, 16 (2007) 1159.
- [6] WANG S.H., PENG J., LUI W.B., ZHANG J.S., *J. Power Sources*, 162 (2006) 486.
- [7] PAULASKAS I.E., BRADY M.P., MEYER III H.M., BUCHANAN R.A., WALKER L.R., *Corr. Sci.*, 48 (2006) 3157.
- [8] EL-ENIM S.A.A., ABDEL-SALAM O.E., EL-ABD H., AMIN A.M., *J. Power Sources*, 177 (2008) 131.
- [9] NIKAM V.V., REDDY R.G., *J. Power Sources*, 152 (2005) 146.
- [10] NIKAM V.V., REDDY R.G., *Electrochim. Acta*, 51 (2006) 6338.
- [11] ANDRE J., ANTONI L., PETIT J.-P., *Int. J. Hydrogen Energy*, 35 (2010) 3684.
- [12] KRAYTSBERG A. AUINAT M., EIN-ELI Y., *J. Power Sources*, 164 (2007) 697.
- [13] HODGSON D.R., MAY B., ADCOCK P.L., DAVIES D.P., *J. Power Sources*, 96 (2001) 233.
- [14] LI M.C., ZENG C.L., LUO S.Z., SHEN J.N., LIN H.C., CAO C.N., *Electrochim. Acta*, 48 (2003) 1735.
- [15] GENG S., LI Y., MA Z., WANG L., WANG F., *J. Power Sources*, 195 (2010) 2356.
- [16] WANG H., SWEIKART M.A., TURNER J.A., *J. Power Sources*, 115 (2003) 243.
- [17] YOON W., HUANG X., FAZZINO P., REIFSNIDER K.L., AKKAOU M.A., *J. Power Sources*, 179 (2008) 265.
- [18] WANG Y., NORTHWOOD D. O., *Electrochim. Acta*, 52 (2007) 6793.
- [19] WANG Y., NORTHWOOD D. O., *J. Power Sources*, 163 (2006) 500.
- [20] FU Y., LIN G., HOU M., WU B., LI H., HAO L., SHAO Z., YI B., *Int. J. Hydrogen Energy*, 34 (2009) 453.
- [21] LARIJANI M.M., YARI M., AFSHAR A., JAFARIAN M., ESHGHABADI M., *J. Alloys and Compounds*, 509 (2011) 7400.
- [22] HUNG Y., EL-KHATIB K.M., TAWFIK H., *J. Applied Electrochemistry*, 35 (2005) 445.
- [23] YAN X., HOU M., ZHANG H., JING F., MING P., YI B., *J. Power Sources*, 160 (2006) 252.
- [24] NAM D.-G., LEE H.-C., *J. Power Sources*, 170 (2007) 268.
- [25] M. WISSLER, *J. Power Sources*, 156 (2006) 142.
- [26] CHUNG C.-Y., CHEN S.-K., CHIN T.-S., KO T.-H., LIN S.-W., CHANG W.-M., HSIAO S.-N., *J. Power Sources*, 186 (2009) 393.
- [27] ZHU J., WANG X., GUO L., WANG Y., WANG Y., YU M., LAU K., *Carbon*, 5 (2007) 2547.
- [28] LARIJANI M. M., YARI M., AFSHAR A., JAFARIAN M., ESHGHABADI M., *J. Alloys and Compounds*, 509 (2011) 7400.
- [29] FUKUTSUKA T., YAMAGUCHI T., MIYANO S.-I., MATSUO Y., SUGIE Y., OGUMI., *J. Power Sources*, 174 (2007) 199.
- [30] WIND J., SPAH R., KAISER W., BOHM G., *J. Power Sources*, 105 (2002) 256.
- [31] KAKATI B.K., YAMSANI V.K., DHATHATHREYAN K.S., SATHIYAMOORTHY D., VERMA A., *Carbon*, 47 (2009), 2413.
- [32] FU Y., LIN G., HOU M., WU B., SHAO Z., YI B., *Int. J. Hydrogen Energy*, 34 (2009) 405.

- [33] DHAKATE S.R., MATHUR R.B., KAKATI B.K., DHAMI T.L., *Int. J. Hydrogen Energy*, 32 (2007), 4537.
- [34] YUAN W., TANG Y., YANG X., WAN Z., *Applied Energy*, 94 (2012) 309.
- [35] ZHANG L., LIU Y., SONG H., WANG S., ZHOU Y., HU S.J., *J. Power Sources*, 162 (2006) 1165.
- [36] WŁODARCZYK R., *Materials Science Forum*, 706-709 (2012), 1047.
- [37] WŁODARCZYK R., DUDEK A., KOBYLECKI R., BIS Z., *Corrosion Resistance, Chapter 9: Corrosion resistance of composites based to graphite used as bipolar plates in fuel cells*, H. Shih – INTECH, Croatia, 2012, p. 189.
- [38] LEE S.-J., HUANG C.-H., LAI J.-J., CHEN Y.-P., *J. Power Sources*, 131 (2004) 162.
- [39] WŁODARCZYK R., WRÓŃSKA A., *Arch. Metall. and Mater.*, 2013, DOI: 10.2478/v10172-012-0156-7.
- [40] WŁODARCZYK R., DUDEK A., NITKIEWICZ Z., *Arch. Metall. and Mater.*, 56 (1), 2011, 182.
- [41] WŁODARCZYK R., KACPRZAK A., KOBYLECKI R., BIS Z., *Functional Materials Letters*, DOI: 10.1142/S1793604713500239.
- [42] WŁODARCZYK R., in press in *Arch. Metall. and Mater.*
- [43] www.iupac.org, website, 2013.
- [44] LEE H.-K., PARK J.-H., KIM D.-Y., LEE T.-H., *J. Power Sources*, 131 (2004) 200.
- [45] GOSTICK J. T., FOWLER M. W., IOANNIDIS M. A., PRITZKER M. D., VOLFKOVICH Y.M., SAKARS A., *J. Power Sources*, 156, (2006) 375.
- [46] MOLIN S., GAZDA M., JASINSKI P., *Solid State Ionics*, 181 (2010) 1214.
- [47] KIM D.-K., LEE D.-G., LEE S., *Metallurgical and Materials Transactions* 32A, (2001) 1111.
- [48] HAKIKI N.E., *J. Applied Electrochemistry*, 40 (2010) 357.
- [49] KRAYTSBERG A., AUNAT M., EIN-ELI., *J. Power Sources*, 164 (2007) 697.
- [50] BARBER M., SUN T.S., PETRACH E., WANG X., ZOU Q., *J. Power Sources*, 185 (2008) 1252.
- [51] CUNNINGHAM B.D., BAIRD D.G., *J. Power Sources*, 168 (2007) 418.
- [52] WŁODARCZYK R., DUDEK A., *Steel Research International*, 81(9), 2010, 1288.

Received 2013-11-27

Accepted 2014-07-03